Quench-induced resonant tunneling mechanisms of bosons in an optical lattice with harmonic confinement

G. M. Koutentakis,[1,2] S. I. Mistakidis,[1] and P. Schmelcher[1,2]

[1]*Zentrum für Optische Quantentechnologien, Universität Hamburg, Luruper Chaussee 149, 22761 Hamburg, Germany*
[2]*The Hamburg Centre for Ultrafast Imaging, Universität Hamburg, Luruper Chaussee 149, 22761 Hamburg, Germany*

The nonequilibrium dynamics of small boson ensembles in a one-dimensional optical lattice is explored upon a sudden quench of an additional harmonic trap from strong to weak confinement. We find that the competition between the initial localization and the repulsive interaction leads to a resonant response of the system for intermediate quench amplitudes, corresponding to avoided crossings in the many-body eigenspectrum with varying final trap frequency. In particular, we show that these avoided crossings can be utilized to prepare the system in a desired state. The dynamical response is shown to depend on both the interaction strength as well as the number of atoms manifesting the many-body nature of the tunneling dynamics.

I. INTRODUCTION

Recent experimental advances in ultracold atomic gases have provided novel ways to examine the static properties and the nonequilibrium dynamics of correlated many-body systems [1–5]. In particular, optical lattice potentials are a prominent feature of ultracold experiments, as they allow for the study of the correlated tunneling dynamics and its dependence on the interparticle interaction [5–9]. Systems consisting of small ensembles of atoms offer the opportunity, both theoretically [8,9] and experimentally [10,11], to identify and track microscopic (quantum) mechanisms due to their finite size and the absence of finite temperature effects. On the other hand, quantum quenches [8,9,12–17] enable us to study the dependence of the dynamical response on the perturbation amplitude applied to an equilibrium system. Therefore, quenched finite systems in combination with the appropriate lattice geometries can lead to new quantum effects, especially when the translational invariance of the lattice is broken.

A well-studied model that breaks the translational invariance consists of a lattice potential with an imposed harmonic trap [5,18–23]. Concerning the dynamics, the ballistic expansion rate of a bosonic Mott insulator trapped in such a composite trap after a quench of the trap frequency to a lower value has been shown to depend on the interparticle interaction [5]. Furthermore, it has been demonstrated [18] that in the limit of low filling factors the dynamics is equivalent to harmonically trapped bosons with a lattice-dependent effective mass. Both of the above-mentioned effects emerge when the harmonic confinement is relatively weak compared to the interparticle repulsion. However, a so far largely unexplored theme is the competition between the harmonic confinement and the interaction strength, which favors different spatial configurations. An intriguing question would therefore be whether this competition can be exploited to obtain a high level of controllability of such a system and, as a consequence, whether the out-of-equilibrium dynamics can be utilized to achieve specific state preparations.

In the present work we consider a small ensemble of bosons confined in an optical lattice subjected to an additional strong harmonic confinement and investigate the dynamics induced by a quench from strong to weak confinement. We first analyze the many-body eigenspectrum for varying trap frequency, revealing the existence of narrow and wide avoided crossings between the many-body eigenstates. The dynamics of the interacting bosons shows distinct regions of weak and strong dynamical response. In particular, for increasing quench amplitude the system exhibits regions of a pronounced response in the vicinity of wide avoided crossings and sharper response peaks being a consequence of the corresponding narrow avoided crossings. Finally, it is shown that we can achieve specific state preparation by utilizing the narrow avoided crossings. Appropriately selecting the postquench trap frequency it is possible to couple the initial state to a desired final one, allowing for a low-frequency and efficient population transfer between the two eigenstates. Finally, the quench-induced many-body dynamics changes significantly with varying particle number and interparticle repulsion, as the positions and widths of the avoided crossings are shifted, giving rise to further variability and controllability of the dynamics. The results presented in this work are obtained by employing the multiconfiguration time-dependent Hartree method for bosons (MCTDHB) [24,25].

The structure of the paper is as follows. In Sec. II we provide the underlying theoretical framework of our work. Section III presents our triple-well results, both for the static case and for the quench-induced dynamics. In Sec. IV we present the generalization of our results for multiwell traps and, finally, in Sec. V we summarize and give an outlook. Appendix describes our computational method.

II. THEORETICAL FRAMEWORK

In the present section we shall briefly discuss our theoretical framework. First, we introduce the many-body Hamiltonian (see Sec. II A) of our system. Then, the wave function representation in terms of a time-independent number state basis (Sec. II B) is outlined. Finally, the basic observables (Sec. II C) used for the interpretation of the dynamics are explained.

A. Hamiltonian

The many-body Hamiltonian of N bosons trapped in a one-dimensional (1D) lattice potential with an imposed harmonic

trap reads

$$H = \sum_{i=1}^{N} \left(-\frac{\hbar^2}{2m}\frac{\partial^2}{\partial x_i^2} + V_0 \sin^2(kx_i) + \frac{m\omega^2}{2}x_i^2 \right)$$
$$+ g\sum_{i=1}^{N}\sum_{j=i+1}^{N}\delta(x_i - x_j), \quad (1)$$

where x_i denotes the position of the ith particle. The optical lattice potential is characterized by its depth V_0 and the corresponding wave number k. The imposed harmonic trap (parallel to lattice axis) depends on its frequency ω and confines the particles around the origin $x = 0$. The effective 1D coupling strength of the contact interaction $g = \frac{2\hbar^2\alpha}{ma_\perp^2}(1 - \frac{|\zeta(1/2)|\alpha}{\sqrt{2}a_\perp})^{-1}$ [26] can be manipulated via the transverse harmonic oscillator length $a_\perp = \sqrt{\frac{\hbar}{M\omega_\perp}}$ (belonging to the strongly confined dimensions) [27,28] or by the 3D s-wave scattering length α via a Feshbach resonance [29,30].

To induce the dynamics we utilize the following scheme: The system is initially prepared in the ground state of the many-body Hamiltonian [see Eq. (1)]. Then, at $t = 0$ we instantaneously change the trap frequency ω to a lower value and let the system evolve under the new Hamiltonian.

Throughout this work we shall employ the recoil energy $E_R = \hbar^2k^2/(2m)$, the inverse wave vector k^{-1} and the bosonic mass m as the units of the energy, length, and mass, respectively. Hard-wall boundary conditions are imposed at $x_\pm = \pm S\pi/2k^{-1}$, where S denotes the number of lattice sites. The depth of the lattice is fixed to $V_0 = 9E_R$, thus including three localized single-particle states.

B. Number state expansion

Using MCTDHB we calculate the many-body wave function $|\Psi(t)\rangle$ with respect to a time-dependent basis consisting of variationally optimized single-particle functions (SPFs), (for more information see Appendix and Refs. [24,25]). However, for the analysis of our results it is preferable to project the numerically obtained $|\Psi(t)\rangle$ in a time-independent number state basis of single-particle states localized on each lattice site. These localized states are constructed using the subset of delocalized eigenstates with b nodes for each lattice site, i.e., $|\psi_i^{(b)}\rangle_{g=0}, i \in \{1, \ldots, S\}$. In the absence of a harmonic confinement this subset of eigenstates belong to the bth Bloch band of the system. To obtain a set of localized states we diagonalize the band-projected position operator $\hat{X}^{(b)} = \hat{P}^{(b)}\hat{x}\hat{P}^{(b)}$, where the operator $\hat{P}^{(b)} = \sum_{k=1}^{S} |\psi_i^{(b)}\rangle_{g=0}\langle\psi_i^{(b)}|_{g=0}$ projects onto the band b [31–33]. In the following, we refer to the eigenstates $|\phi_s^{(b)}\rangle, s \in \{1, \ldots, S\}$ of $\hat{X}^{(b)}$ as the single-band Wannier states of the deformed lattice. The corresponding N-body number state basis reads

$$\left|\bigotimes_{b_1} n_1^{(b_1)}, \ldots, \bigotimes_{b_S} n_S^{(b_S)}\right\rangle = \sum_{i=1}^{N!} \frac{\hat{\mathcal{P}}_i\left(\bigotimes_{j=1}^{N}|\phi_{s_j}^{(b_j)}\rangle\right)}{\sqrt{N!\prod_{b,s}n_s^{(b)}!}}, \quad (2)$$

where the operator $\hat{\mathcal{P}}_i$ performs the ith permutation of N elements and $n_s^{(b)}$ refers to the number occupation of the Wannier state $|\phi_s^{(b)}\rangle$. To simplify the notation we shall make the

following assumptions. We omit the superscript if no Wannier state or only the Wannier states belonging to the zeroth band are occupied, and decompose the occupation number as $n^{(b_1)} \otimes n^{(b_2)} \otimes \cdots$ if more than a single Wannier state localized in a certain well is occupied. For instance, $|1^{(0)}, 1^{(0)} \otimes 1^{(1)}, 1^{(2)}\rangle$ refers to the four-particle state of the triple-well where the ground states of the left and the middle well, the first excited state of the middle well, as well as the second excited state of the right well are each occupied by one boson. For later convenience we also denote by $|\vec{n}\rangle_S$ ($|\vec{n}\rangle_A$) the parity symmetric (antisymmetric) combination of the states $|\vec{n}\rangle = |\otimes n_1, \otimes n_2, \ldots, \otimes n_S\rangle$ and $|\otimes n_S, \otimes n_{S-1} \ldots, \otimes n_1\rangle$.

In the presence of a harmonic confinement, the Wannier number states are not uniquely ordered with respect to their energy expectation value, as argued in the following. Indeed, let us consider a system of four bosons in a triple well. For strong harmonic confinement and $g = 0$ there are five number state subsets: $h_0 = \{|0,4,0\rangle\}, h_1 = \{|1,3,0\rangle_{S,A}\}, h_2 = \{|2,2,0\rangle_{S,A}, |1,2,1\rangle\}, h_3 = \{|3,1,0\rangle_{S,A}, |2,1,1\rangle_{S,A}\}$, and $h_4 = \{|4,0,0\rangle_{S,A}, |3,0,1\rangle_{S,A}, |2,0,2\rangle\}$ ordered in increasing energy. On the other hand, for an interacting gas with vanishing harmonic confinement there are four subsets of number states energetically ordered by the multiplicity of bosons that reside in each well: single pairs $i_{SP} = \{|2,1,1\rangle, \circlearrowleft\}$, double pairs $i_{DP} = \{|2,2,0\rangle, \circlearrowleft\}$, triplets $i_T = \{|3,1,0\rangle, \circlearrowleft\}$, and quadruplets $i_Q = \{|4,0,0\rangle, \circlearrowleft\}$, where $\circlearrowleft$ stands for site permutations. Note that, for interaction energies of the order of the band gap, also higher band excitations must be considered.

From the above example it becomes evident that a reordering of the number states in energy takes place as the system passes from the one limiting case to the other. For instance, the state $|0,4,0\rangle$ belonging to the classes h_0 and i_Q, is the most favorable state for strong confinement but, at the same time, the most unfavorable for strong interactions. As we shall see, this corresponding reordering process is the main reason for the resonant dynamics in the quenched system.

C. Observables

Let us now briefly introduce a few basic observables to be utilized in the following analysis, which are based on the one-body density $\rho^{(1)}(x;t)$. To quantify the time evolution of interwell and intrawell modes we use the average position of the bosons in a spatial region $D, D = \{x \in (x_i, x_f)\}$

$$\langle x\rangle_D(t) = \langle\Psi(t)|\hat{x}_D|\Psi(t)\rangle = \frac{1}{N_D}\int_{x_i}^{x_f}dx\, x\rho^{(1)}(x;t), \quad (3)$$

where $N_D = \int_{x_i}^{x_f}dx\rho^{(1)}(x;t)$ is the particle number within D, $\hat{x}_D = \int_{x_i}^{x_f}dx\, x\hat{\Psi}^\dagger(x)\hat{\Psi}(x)$ refers to a one-body operator, and $\hat{\Psi}(x)$ is the field operator. This quantity offers a measure for the collective displacement of the atoms (see Ref. [34] for the dipole mode) within a prescribed region of the lattice.

Further, we introduce the position variance in a spatial region D

$$\sigma_{x,D}^2(t) = \langle\Psi(t)|\hat{x}_D^2|\Psi(t)\rangle - \langle\Psi(t)|\hat{x}_D|\Psi(t)\rangle^2$$
$$= \frac{1}{N_D}\int_{x_i}^{x_f}dx\, x^2\rho^{(1)}(x;t) - \langle x\rangle_D^2(t), \quad (4)$$

which measures the expansion and contraction of the atomic cloud (see Ref. [35] for the breathing mode) within D. Note the appearance of the one-body operator $\hat{x}_D^2 = \int_{x_i}^{x_f} dx\, x^2 \hat{\Psi}^\dagger(x)\hat{\Psi}(x)$. The position variance over the whole lattice $\sigma_{x,L}^2(t)$ quantifies a global breathing mode, composed of intersite tunneling and intrasite breathing and dipole modes, which contribute altogether to the total contraction and expansion of the atomic cloud. $\sigma_{x,L}^2(t)$ thus offers a measure for the net dynamical response of the system.

To measure the impact of the quench we also define the time-averaged position variance

$$\overline{\sigma_{x,L}^2} - \sigma_{x,L}^2(0) \equiv \frac{1}{T}\int_0^T dt\left[\sigma_{x,L}^2(t) - \sigma_{x,L}^2(0)\right]$$
$$\underset{T\to\infty}{=} \sum_{i>j} \mathrm{Re}\left(c_i^* {}_\omega\langle\Psi_i|\hat{x}_L^2|\Psi_j\rangle_\omega c_j\right), \quad (5)$$

which describes how far the system is in average from its initial state. Here, $|\Psi_i\rangle_\omega$ is the ith excited stationary eigenstate of the postquench Hamiltonian and $|\Psi\rangle = \sum_i c_i |\Psi_i\rangle_\omega$ holds. We have also used the parity symmetry, which implies $\langle x\rangle_L(t) = \langle x\rangle_L(0) = 0$ (since the initial state is the ground state of the Hamiltonian before the quench). Finally, the temporal variance of the position variance

$$\Delta_T\{\sigma_{x,L}^2\} \equiv \frac{1}{T}\int_0^T dt\left(\sigma_{x,L}^2(t) - \overline{\sigma_{x,L}^2}\right)^2$$
$$\underset{T\to\infty}{=} \frac{1}{2}\sum_{i>j}\left|c_i^* {}_\omega\langle\Psi_i|\hat{x}_L^2|\Psi_j\rangle_\omega c_j\right|^2 \quad (6)$$

quantifies how much the state fluctuates around its average configuration during the evolution. $\Delta_T\{\sigma_{x,L}^2\}$ thus measures the intensity of the dynamical processes and of defect formations following a quench. The theoretical limit $T \to \infty$ is replaced in practice by a finite evolution time T where $\overline{\sigma_{x,L}^2}$ and $\Delta_T\{\sigma_{x,L}^2\}$ have converged.

III. QUENCH DYNAMICS WITHIN A TRIPLE WELL

As a prototype system exhibiting characteristic quench-induced dynamics, we use a system of four harmonically trapped bosons in a triple-well potential. We first investigate the eigenspectra of the system with varying trap frequency (Sec. III A), which are subsequently related to the dynamics induced by the quench (Sec. III B).

A. Eigenspectra

The eigenstate spectrum of the Hamiltonian of Eq. (1) depends on both the trap frequency ω and the interaction strength g (see also Sec. II B). To interpret the dynamics caused by a quench of the frequency ω of the imposed harmonic trap we analyze how the eigenstate spectrum depends on ω.

Figure 1(a) shows the ω dependence of the eigenenergies for $g = 1E_R k^{-1}$. For later convenience we denote each of the even-parity eigenstates as $|\Psi_i\rangle$, where $i \in \{0,\ldots,8\}$ refers to their energetical order for a given ω. In the following, we focus on the even-parity part of the spectrum $|\Psi_i\rangle$ [see Fig. 1(a)], which contains the ground state $|\Psi_0\rangle$. At $\omega = 0$ the number states within each class (i_X, $X = SP, DP, T, Q$) are very close
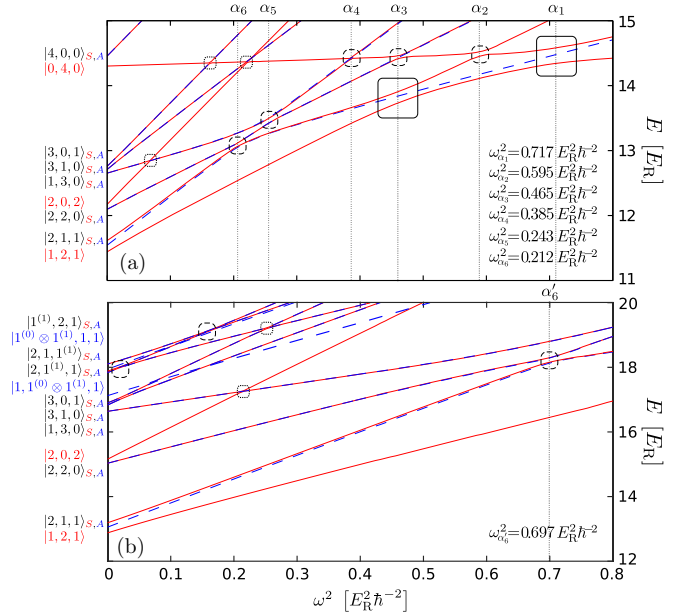

FIG. 1. Dependence of the eigenenergies of the Hamiltonian of Eq. (1) on the trap frequency ω^2 for a system consisting of $N = 4$ bosons trapped in a triple well with additional harmonic confinement. The lowest (a) 15 eigenenergies for $g = 1E_R k^{-1}$ and (b) 20 eigenenergies for $g = 4E_R k^{-1}$ are shown. Solid (dashed) lines represent even (odd) parity eigenstates. Very narrow crossings (width smaller than $4\times 10^{-3} E_R^2 \hbar^{-2}$) are denoted by dotted boxes, narrow avoided crossings are indicated by dashed boxes and wide avoided crossings are denoted by solid boxes. α_i, $i = 1,\ldots,6$ indicate the position of each avoided crossing (see legend). The dominant number state contribution of each eigenstate at $\omega = 0$ is indicated on the left-hand side of each figure.

in energy, their minor energetical difference being caused by the respective avoided crossings (and the boundary conditions of the triple well), and thus the eigenstates are a superposition of the corresponding Wannier number states. In particular, each of the eigenstates possesses a dominant contribution from a particular Wannier number state of class i_X [presented on the left-hand side of Fig. 1(a)]. For $\omega > 0$, the eigenenergies increase linearly (proportional to the number of bosons in the side wells) with ω^2. The population of the dominant contribution of each eigenstate increases with ω^2 (at the expense of the contribution of other number states that belong to the same class) up to the point of complete dominance and therefore saturation. This behavior with increasing ω^2 occurs unless we encounter an avoided crossing with another eigenstate. Indeed, as it can be seen in Fig. 1(a) at such avoided crossings (being denoted by $C \in \{\alpha_i\}$, $i = 1,\ldots,6$) the two involved eigenstates exchange their character and therefore corresponding dominant Wannier number states. Indicative of this process is the fact that for $\omega^2 > \omega_C^2$ the linear ω^2 dependence of the eigenstates is restored and the corresponding slopes have been exchanged. Moreover, the avoided crossings α_6 and α_5 due to their proximity exhibit a slightly different behavior being referred to in the following as a composite avoided crossing $\{\alpha_6\alpha_5\}$. We note that the avoided crossings, which involve the ground state $|\Psi_0\rangle$ are much wider (wide avoided crossings) compared to those involving excited

states (narrow avoided crossings). Despite the appearance of the above-mentioned avoided crossings there are also very narrow avoided crossings possessing a corresponding width smaller than $4 \times 10^{-3} E_R^2 \hbar^{-2}$.

To interpret the eigenspectrum we employ the corresponding (three-site, lowest-band) Bose-Hubbard model (BHM) [36,37]

$$\hat{H}_{BHM} = -J(\hat{a}_1^\dagger \hat{a}_2 + \hat{a}_2^\dagger \hat{a}_3 + \text{H.c.}) + \sum_{i=1}^{3} [\epsilon(i-2)^2 + e_0]\hat{n}_i$$

$$+ \frac{U}{2} \sum_{i=1}^{3} \hat{n}_i(\hat{n}_i - 1), \tag{7}$$

where $\hat{a}_i$ ($\hat{a}_i^\dagger$) denotes the annihilation (creation) operator that annihilates (creates) a particle in the state $|\phi_i^{(0)}\rangle$ (e.g., $i = 1$ refers to the leftmost well) and $\hat{n}_i = \hat{a}_i^\dagger \hat{a}_i$ corresponds to the particle number operator. The Hubbard parameters J, U, ϵ, and e_0 refer to the intersite hopping, intrasite interaction, site offset energy, and the zero point energy of the ensemble, respectively. We remark that all of the presented results are obtained within the MCTDHB framework for the continuum space Hamiltonian of Eq. (1) and we only refer to discrete models [BHM, see Eq. (7)], to interpret and compare our findings.

The classification in terms of the interparticle interaction (i_X) provides information on the energy expectation value of the corresponding states for a vanishing harmonic confinement. Furthermore, the classification in terms of strong harmonic confinement provides information on how the energy of each Wannier number state depends on the trap frequency, i.e., $E\{h_d\}(\omega) = E\{h_d\}|_{\omega=0} + d\epsilon$ ($\epsilon \propto \omega^2$). For instance, at $J = 0$ all the crossings become exact [since all individual n_i are conserved, see Eq. (7)] and we can evaluate the expected position for each one, e.g., the states $|1,2,1\rangle$ and $|1,3,0\rangle_S$ are expected to cross at $\epsilon = 4U$. For $J \neq 0$ these exact crossings become avoided and their widths can be approximated by the coupling between the involved states, e.g., $\langle 1,2,1|\hat{H}_{BHM}|1,3,0\rangle_S = -\sqrt{3/2}J$, [see the wide avoided crossing in Fig. 1(a) at $\omega^2 = \omega_{\alpha_3}^2$]. Narrow avoided crossings emerge from higher order transitions yielding a nonlinear coupling in J, e.g., although $\langle 0,4,0|\hat{H}_{BHM}|1,2,1\rangle = 0$ these states are coupled by the higher-order transition $|0,4,0\rangle \overset{J}{\rightleftharpoons} |1,3,0\rangle_S \overset{J}{\rightleftharpoons} |1,2,1\rangle$ leading to a coupling $\propto J^2$. Here, the hopping $J \ll U$, and therefore the corresponding avoided crossing observed at $\omega^2 = \omega_{\alpha_2}^2$ [see Fig. 1(a)] is much narrower. On the other hand, the composite avoided crossing $\{\alpha_6 \alpha_5\}$ can be interpreted as follows: At $\omega_{\alpha_6}^2$ a comparatively narrow avoided crossing between the eigenstates $|\Psi_1\rangle$ and $|\Psi_2\rangle$ takes place (exchange between the Wannier number states $|2,1,1\rangle_S$ and $|2,2,0\rangle_S$). A wide avoided crossing involving the eigenstates $|\Psi_1\rangle$ and $|\Psi_3\rangle$ follows at $\omega_{\alpha_6}^2 \leqslant \omega^2 \leqslant \omega_{\alpha_5}^2$ (exchange between the Wannier number states $|1,3,0\rangle_S$, $|2,1,1\rangle_S$). Finally, at $\omega_{\alpha_5}^2$ a second narrow avoided crossing takes place between the eigenstates $|\Psi_2\rangle$ and $|\Psi_3\rangle$ (exchange between the number states $|2,1,1\rangle_S$ and $|2,2,0\rangle_S$). This behavior stems from the fact that all these three states are degenerate for $J = 0$, $\epsilon = U$, while for finite J the coupling between $|2,1,1\rangle_S$ and $|1,3,0\rangle_S$ can

be neglected. To connect our Hamiltonian [Eq. (1)] with the employed BHM [see Eq. (7)] we mention here that the studied case of $V_0 = 9E_R$ and $g = 1E_R k^{-1}$ corresponds to the BHM Hamiltonian with parameters $U \sim 0.13E_R$, $J \sim 1.5 \times 10^{-2} E_R$, yielding a ratio $U/J \sim 8.5$. The offset induced by the imposed harmonic oscillator potential corresponds to $\epsilon/\omega^2 \sim 0.55\hbar^2/E_R$. Finally, it can be shown that the energy of the $|0,4,0\rangle$ state depends on the trap frequency as $\sim 1 + \frac{\omega^2}{4V_0}$, related to the zero point energy e_0 [see Eq. (7)].

For larger interaction strength, the many-body states, as shown in Fig. 1(b), become energetically higher due to the higher interaction energy among the bosons. Note that a certain number of states with higher band excitations possess lower energies from states of the lowest band, e.g., the state $|0,4,0\rangle$ does not participate in the lowest twenty eigenstates of the Hamiltonian with $g = 4E_R k^{-1}$ [see Fig. 1(b)]. Indeed, for $g = 4E_R k^{-1}$ the BHM can still be applied since: (i) there is no coupling to higher band excitations via hopping terms of the form $-J_{ij}^{b,b'} a_i^{\dagger(b)} a_j^{(b')} = 0$ due to the orthogonality of the single-particle Bloch states that belong to different bands, and (ii) in the interaction part of the Hamiltonian, intraband on-site interaction terms due to $U_{i,i,i,i}^{b,b,b,b} a_i^{\dagger(b)} a_i^{\dagger(b)} a_i^{(b)} a_i^{(b')}$, where $|b - b'| = 2j + 1$, $j \in \mathbb{N}$ vanish because of parity symmetry within the corresponding well [38]. This manifests itself in Fig. 1(b) by the absence of avoided crossings between states with higher band excitations (first excited band) and states with all particles in the zeroth band (see, for instance, the very narrow avoided crossing at $\omega^2 = 0.25E_R^2 \hbar^{-2}$ involving the states $|\Psi_7\rangle$ and $|\Psi_8\rangle$). The energies of the latter possess a similar dependence on the frequency ω^2 as for $g = 1E_R k^{-1}$ but the position in terms of ω^2 of the avoided crossings between these states [see Fig. 1(a)] has increased approximately three times the original value for $g = 1E_R k^{-1}$. The dependence of the eigenenergies involving higher band excitations is linear in ω^2 with the proportionality factor $\epsilon^{(1)} = \epsilon$, see for instance $|\Psi_0\rangle$ and $|\Psi_8\rangle$ within the frequency interval $\omega^2 \in [0.1, 0.25E_R^2 \hbar^{-2}]$. Furthermore, the states with higher band excitations show both narrow and wide avoided crossings, e.g., see the narrow avoided crossing at $\omega^2 = 0.02E_R^2 \hbar^{-2}$ involving the states $|\Psi_8\rangle$ and $|\Psi_9\rangle$ and the wide avoided crossing at $\omega^2 \in [0.02, 0.16E_R^2 \hbar^{-2}]$ between the states $|\Psi_8\rangle$ and $|\Psi_{10}\rangle$. The narrow avoided crossings refer to intraband tunneling within the ground band while the wide avoided crossings are related to interband tunneling within the first excited band. Finally, let us also note that the narrow avoided crossings between (the parity symmetric) states with higher band excitations comprise a composite avoided crossing [see the dashed boxes at $\omega^2 \sim 0.02E_R^2 \hbar^{-2}$ and $\omega^2 \sim 0.16E_R^2 \hbar^{-2}$ in Fig. 1(b)] similar to the $\{\alpha_6 \alpha_5\}$ avoided crossing observed for the ground band [see Fig. 1(a)].

Non-negligible widths of avoided crossings between states of the ground band and those having a contribution from the first excited band can in principle be achieved by shifting the center of the harmonic trap. This is equivalent to a lattice tilt [39] where the parity symmetry of the system is broken and states of different parity become coupled. According to Figs. 1(a), 1(b) the states with different parity, e.g., $|\vec{n}\rangle_S$ and $|\vec{n}\rangle_A$ are near degenerate, except for the case of avoided crossings, and consequently we expect that the spectrum is slightly altered for the case of broken parity symmetry.
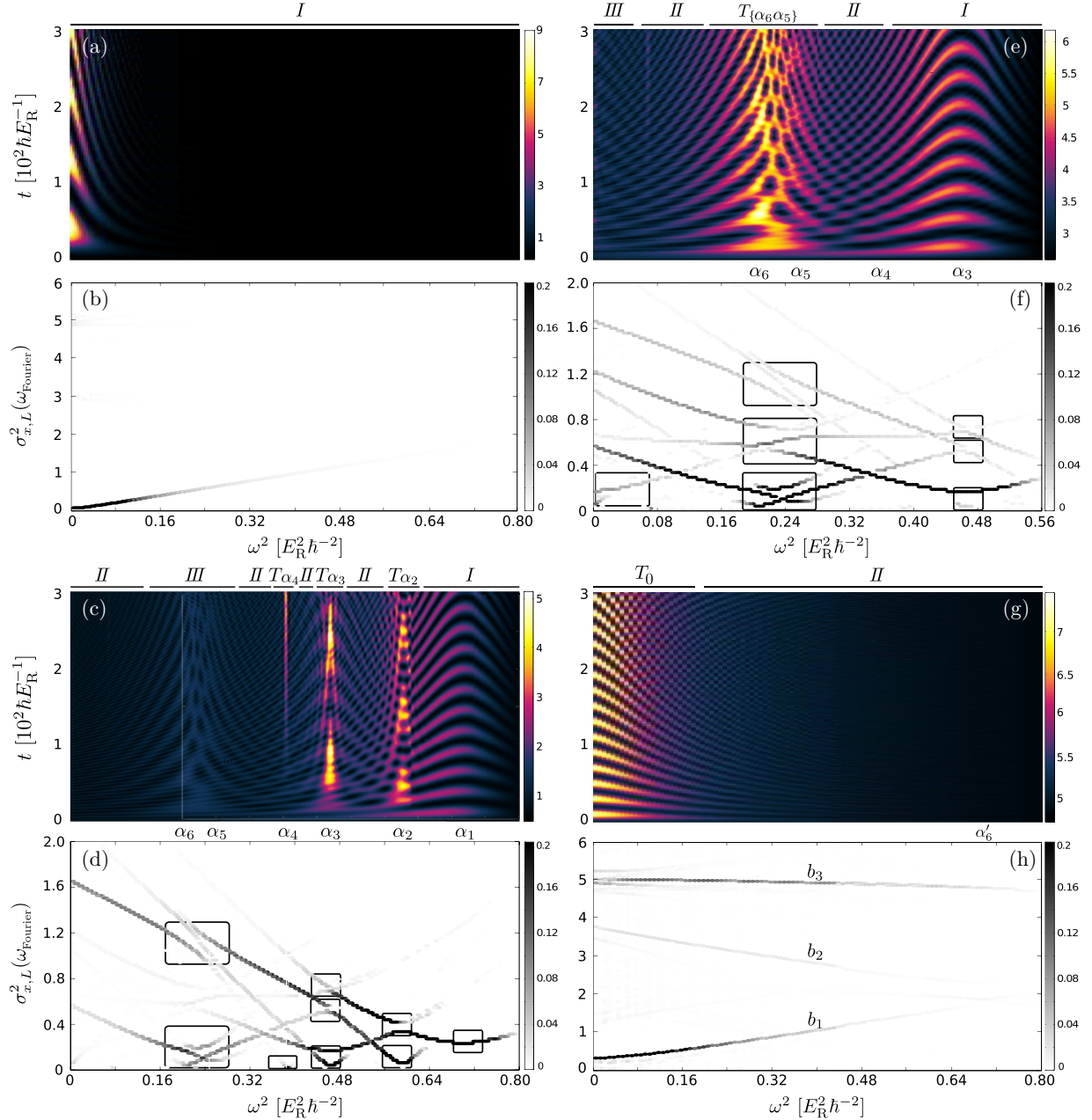
FIG. 2. (a), (c), (e), (g) Time evolution of $\sigma_{x,L}^2(t)$ and (b), (d), (f), (h) the corresponding spectra $\sigma_{x,L}^2(\omega_{\text{Fourier}})$, as a function of the trap frequency ω^2 after the quench. The system parameters used in each case correspond to (a), (b) $g = 0 E_R k^{-1}$, $\omega_i^2 = 0.8 E_R^2 \hbar^{-2}$ (initial trap frequency), (c), (d) $g = 1 E_R k^{-1}$, $\omega_i^2 = 0.8 E_R^2 \hbar^{-2}$, (e), (f) $g = 1 E_R k^{-1}$, $\omega_i^2 = 0.58 E_R^2 \hbar^{-2}$, and (g), (h) $g = 4 E_R k^{-1}$, $\omega_i^2 = 0.8 E_R^2 \hbar^{-2}$. α_i, $i = 1, \ldots, 6$ denote the positions of the corresponding avoided crossings (see also Fig. 1). Note that on top of each of the (a), (c), (e), (h) subfigures regions I, II, III, T_C with $C \in \{\alpha_i\}$, are presented. In (d), (f) the branches are organized by solid boxes denoted in Table I as segment $\alpha_{i,j}$, where the index $j = 1, 2, 3$ introduces an energetically increasing order.

B. Quench-induced dynamics

After having examined the basic properties of the eigenstate spectrum we proceed by investigating the many-body dynamics when the system is subjected to an abrupt quench of the trap frequency ω to lower values.

For a strongly confined system initialized in the noninteracting ground state ($|\Psi\rangle \sim \prod |\phi_c^{(0)}\rangle$, c stands for the middle well) the dynamical response of the system (for varying final trap frequency ω) is shown in Fig. 2(a) via $\sigma_{x,L}^2(t)$ [see Eq. (4)]. This response can be described by the two single-particle

states, i.e., by $|\phi_c^{(0)}\rangle$ and the symmetric state $\frac{1}{\sqrt{2}}(|\phi_r^{(0)}\rangle + |\phi_\ell^{(0)}\rangle)$ (l, r stand for the left and right wells respectively). For $\omega^2 > 0.08 E_R^2 \hbar^{-2}$ we have $\sigma_{x,L}^2(t) \approx \sigma_{x,L}^2(0)$ showing that the system is unaffected by the quench and all the particles remain essentially localized in the center well ($\sim |\phi_c^{(0)}\rangle$). Only for quenches to very low trapping frequencies $\omega^2 < 0.08 E_R^2 \hbar^{-2}$, see in Fig. 2(a) the particles diffuse to the outer wells and as a consequence the variance fluctuates significantly with time. The spectrum of the variance $\sigma_{x,L}^2(\omega_{\text{Fourier}})$, presented in Fig. 2(b), is dominated by a single frequency for all quenches,

TABLE I. Energy differences and the corresponding main tunneling processes for each branch that appear in the spectra of Fig. 2(d), 2(f). Each avoided crossing is denoted by $\alpha_i, i = 1, \ldots, 6$, while 0 refers to the avoided crossings located at $\omega = 0$. The branches are categorized into segments being denoted by a second subscript index j, i.e., $\alpha_{i,j}, j = 1, 2, 3$. The energy difference of a given branch is denoted by $E_{km} \equiv E_k - E_m$ followed by the corresponding main tunneling processes and the respective frequency domains.

	$\{\alpha_6\alpha_5\}$			α_3			α_2	
$\{\alpha_6\alpha_5\}_1$	$E_{21}\begin{vmatrix}\lvert1,3,0\rangle_S \rightleftharpoons \lvert2,2,0\rangle_S \\ \lvert2,1,1\rangle_S \rightleftharpoons \lvert2,2,0\rangle_S\end{vmatrix}$	$\begin{matrix}\omega^2 > \omega^2_{\alpha_5} \\ \omega^2 < \omega^2_{\alpha_5}\end{matrix}$	$\alpha_{3,1}$	$E_{32}\ \lvert2,2,0\rangle_S \rightleftharpoons \lvert0,4,0\rangle$ $E_{10}\ \lvert1,3,0\rangle_S \rightleftharpoons \lvert1,2,1\rangle$	$\omega^2 \approx \omega^2_{\alpha_3}$ $\omega^2 \approx \omega^2_{\alpha_3}$	$\alpha_{2,1}$	$E_{21}\ \lvert1,2,1\rangle \rightleftharpoons \lvert0,4,0\rangle$	$\omega^2 \approx \omega^2_{\alpha_2}$
	$E_{32}\begin{vmatrix}\lvert2,1,1\rangle_S \rightleftharpoons \lvert2,2,0\rangle_S \\ \lvert1,3,0\rangle_S \rightleftharpoons \lvert2,2,0\rangle_S\end{vmatrix}$	$\begin{matrix}\omega^2 > \omega^2_{\alpha_6} \\ \omega^2 < \omega^2_{\alpha_6}\end{matrix}$						
	$E_{31}\lvert1,3,0\rangle_S \rightleftharpoons \lvert2,2,0\rangle_S$	$\omega^2 \in (\omega^2_{\alpha_6}, \omega^2_{\alpha_5})$						
$\{\alpha_6\alpha_5\}_2$	$E_{10}\begin{vmatrix}\lvert1,3,0\rangle_S \rightleftharpoons \lvert1,2,1\rangle \\ \lvert2,1,1\rangle_S \rightleftharpoons \lvert1,2,1\rangle\end{vmatrix}$	$\begin{matrix}\omega^2 > \omega^2_{\alpha_6} \\ \omega^2 < \omega^2_{\alpha_6}\end{matrix}$	$\alpha_{3,2}$	$E_{21}\begin{vmatrix}\lvert2,2,0\rangle_S \rightleftharpoons \lvert1,3,0\rangle_S \\ \lvert0,4,0\rangle \ \ \rightleftharpoons \lvert1,2,1\rangle\end{vmatrix}$	$\begin{matrix}\omega^2 < \omega^2_{\alpha_3} \\ \omega^2 > \omega^2_{\alpha_3}\end{matrix}$	$\alpha_{2,2}$	$E_{10}\begin{vmatrix}\lvert1,3,0\rangle_S \rightleftharpoons \lvert0,4,0\rangle \\ \lvert1,3,0\rangle_S \rightleftharpoons \lvert1,2,1\rangle\end{vmatrix}$	$\begin{matrix}\omega^2 > \omega^2_{\alpha_2} \\ \omega^2 < \omega^2_{\alpha_2}\end{matrix}$
	$E_{20}\begin{vmatrix}\lvert2,1,1\rangle_S \rightleftharpoons \lvert1,2,1\rangle \\ \lvert2,2,0\rangle_S \rightleftharpoons \lvert1,2,1\rangle\end{vmatrix}$	$\begin{matrix}\omega^2 \in (\omega^2_{\alpha_6}, \omega^2_{\alpha_5}) \\ \omega^2 \notin (\omega^2_{\alpha_6}, \omega^2_{\alpha_5})\end{matrix}$		$E_{31}\lvert1,3,0\rangle_S \rightleftharpoons \lvert0,4,0\rangle$	$\omega^2 < \omega^2_{\alpha_3}$		$E_{20}\begin{vmatrix}\lvert1,3,0\rangle_S \rightleftharpoons \lvert1,2,1\rangle \\ \lvert1,3,0\rangle_S \rightleftharpoons \lvert0,4,0\rangle\end{vmatrix}$	$\begin{matrix}\omega^2 > \omega^2_{\alpha_2} \\ \omega^2 < \omega^2_{\alpha_2}\end{matrix}$
	$E_{30}\begin{vmatrix}\lvert2,1,1\rangle_S \rightleftharpoons \lvert1,2,1\rangle \\ \lvert1,3,0\rangle_S \rightleftharpoons \lvert1,2,1\rangle\end{vmatrix}$	$\begin{matrix}\omega^2 > \omega^2_{\alpha_5} \\ \omega^2 < \omega^2_{\alpha_5}\end{matrix}$						
$\{\alpha_6\alpha_5\}_3$	$E_{43}\lvert1,3,0\rangle_S \rightleftharpoons \lvert0,4,0\rangle$ $E_{42}\lvert1,3,0\rangle_S \rightleftharpoons \lvert0,4,0\rangle$ $E_{41}\lvert1,3,0\rangle_S \rightleftharpoons \lvert0,4,0\rangle$	$\omega^2 < \omega^2_{\alpha_5}$ $\omega^2 \in (\omega^2_{\alpha_6}, \omega^2_{\alpha_5})$ $\omega^2 > \omega^2_{\alpha_6}$	$\alpha_{3,3}$	$E_{20}\begin{vmatrix}\lvert1,3,0\rangle_S \rightleftharpoons \lvert0,4,0\rangle \\ \lvert2,2,0\rangle_S \rightleftharpoons \lvert1,2,1\rangle\end{vmatrix}$ $E_{30}\lvert1,2,1\rangle \ \ \rightleftharpoons \lvert0,4,0\rangle$	$\begin{matrix}\omega^2 > \omega^2_{\alpha_3} \\ \omega^2 < \omega^2_{\alpha_3}\end{matrix}$ $\omega^2 < \omega^2_{\alpha_3}$			

	α_4			α_1			0	
$\alpha_{4,1}$	$E_{43}\ \lvert2,1,1\rangle_S \rightleftharpoons \lvert0,4,0\rangle$	$\omega^2 \approx \omega^2_{\alpha_4}$	$\alpha_{1,1}$	$E_{10}\ \lvert1,3,0\rangle_S \rightleftharpoons \lvert0,4,0\rangle$	$\omega^2 \approx \omega^2_{\alpha_1}$	$0_{1,1}$	$E_{10}\ \lvert2,1,1\rangle_S \rightleftharpoons \lvert1,2,1\rangle$ $E_{23}\ \lvert2,2,0\rangle_S \rightleftharpoons \lvert2,0,2\rangle$	$\omega \approx 0$ $\omega \approx 0$

and this frequency corresponds to the Rabi frequency involving the energy difference between the two aforementioned states.

Figure 2(c) presents $\sigma^2_{x,L}(t)$ as a function of ω^2 for intermediate interactions $g = 1 E_R k^{-1}$. Here, the ground state is dominated by the $\lvert0,4,0\rangle$ number state for the initial trap frequency $\omega^2_i = 0.8$ [see Fig. 1(a)]. Regions of qualitatively different dynamical response with varying final trap frequency ω^2 are manifest, denoted as I, II, III, and T_C in Fig. 2(c), thereby showing also a prominent difference from the $g = 0$ case [see Fig. 2(a)]. Within the region denoted as type I ($\omega^2 > \omega^2_{\alpha_2}$) $\sigma^2_{x,L}(t)$ fluctuates prominently with time, indicating the presence of the global breathing mode. Here the fluctuations of $\sigma^2_{x,L}(t)$ are still characterized by a single frequency [see Fig. 2(d)], and correspond to the Rabi oscillation region studied also in Ref. [18]. The regions of type T_C (associated with a corresponding avoided crossing C) are characterized by a small frequency and high-amplitude response during the evolution. Regions of type II appear in between regions of type T_C, e.g., $\omega^2_{\alpha_3} < \omega^2 < \omega^2_{\alpha_2}$. Here, the variance $\sigma^2_{x,L}(t)$ evolves with a multitude of frequencies while its amplitude is diminished compared to the case of regions I and T. Finally, within the region II a region III (linked to the composite avoided crossing $\{\alpha_6\alpha_5\}$) of relatively strong response emerges.

To gain more insight into the existence of the regions II, III, and T_C, we employ $\sigma^2_{x,L}(\omega_{\text{Fourier}})$ shown in Fig. 2(d). The connection of each of the branches observed in Fig. 2(d) to the related eigenenergy differences is presented in detail in Table I. We remark that only branches involving the state $\lvert0,4,0\rangle$ (being the dominant Wannier number state contribution of the initial state) are contributing significantly. The region I is formed due to the avoided crossing α_1 [see Fig. 1(a)] and the bosons perform Rabi tunneling oscillations between the number states

$\lvert0,4,0\rangle$ and $\lvert1,3,0\rangle_S$ (see segment $\alpha_{1,1}$ in Table I). Turning to the region T_{α_2} we observe that the dynamical response of the system is dominated by the low-frequency second-order tunneling process $\lvert1,2,1\rangle \rightleftharpoons \lvert0,4,0\rangle$ (see segment $\alpha_{2,1}$ in Table I). The formation of regions II ($\omega^2_{\alpha_3} \leqslant \omega^2 \leqslant \omega^2_{\alpha_2}$) is caused by the fact that the tunneling modes $\lvert1,2,1\rangle \rightleftharpoons \lvert0,4,0\rangle$, $\lvert1,3,0\rangle_S \rightleftharpoons \lvert1,2,1\rangle$, and $\lvert1,3,0\rangle_S \rightleftharpoons \lvert0,4,0\rangle$ (see segments $\alpha_{2,1}$ and $\alpha_{2,2}$ in Table I) possess a similar amplitude [see also Fig. 2(d)] and the interference of these modes is destructive (on average) resulting in a weakened dynamical response. At T_{α_3} ($\omega^2 = \omega^2_{\alpha_3}$) a low-frequency second-order tunneling mode $\lvert2,2,0\rangle_S \rightleftharpoons \lvert0,4,0\rangle$ (see segment $\alpha_{3,1}$ in Table I) is observed. For larger quenches, i.e., $\omega^2 < \omega^2_{\alpha_3}$, the eigenstate dominated by $\lvert0,4,0\rangle$ does not couple with the remaining states of the eigenspectrum [see also Fig. 1(a)]. Then, most of the processes appearing within this trap frequency regime are associated with the small $\lvert1,3,0\rangle_S$ contribution to the initial state. The above give rise to the region II which encompasses the T_{α_4} and III regions. The T_{α_4} region is dominated by a low-frequency mode being the third-order process $\lvert2,1,1\rangle_S \rightleftharpoons \lvert0,4,0\rangle$ (see segment $\alpha_{4,1}$). Note that even for very low detuning ($\omega^2 \neq \omega^2_{\alpha_4}$) from the crossing α_4, this third-order process vanishes because: (i) the width of the avoided crossing α_4 is extremely narrow and (ii) the state $\lvert2,1,1\rangle_S$ has no contribution to the initial state. Finally, within the region III that appears near the crossing $\{\alpha_6\alpha_5\}$ [see Figs. 2(c), 2(d)] the relevant low-frequency tunneling processes are $\lvert2,1,1\rangle_S \rightleftharpoons \lvert2,2,0\rangle_S$ and $\lvert1,3,0\rangle_S \rightleftharpoons \lvert2,2,0\rangle_S$ (see segment $\{\alpha_6\alpha_5\}_1$ in the appropriate regions and also Table I). Here, the prominent dynamics of the state $\lvert1,3,0\rangle_S$ gives rise to a slightly increased response of the system in comparison to region II.

To examine the case of the composite avoided crossing $\{\alpha_6\alpha_5\}$ we initialize the system to the ground state $\lvert\Psi_0\rangle$

($g = 1E_R k^{-1}$ and $\omega_i^2 = 0.560 E_R^2 \hbar^{-2}$) being dominated by the Wannier number state $|1,3,0\rangle_S$. Figure 2(e) shows $\sigma_{x,L}^2(t)$ for different final trapping frequencies ω. For $\omega^2 > \omega_{\alpha_4}^2$ the system undergoes Rabi oscillations of varying amplitude [region I in Fig. 2(e)]. As the quench amplitude increases the system transits smoothly via the region II where the amplitude of the Rabi oscillations decreases to the region $T_{\{\alpha_6 \alpha_5\}}$ where the response of the system is prominent. Note here that the region $T_{\{\alpha_6 \alpha_5\}}$ is broader than the previously mentioned regions of type T_C. Finally, for $\omega^2 < \omega_{\alpha_6}^2$ (region II) the response of the system becomes multimode and the fluctuations of $\sigma_{x,L}^2(t)$ are diminished.

To identify the corresponding microscopic processes, Fig. 2(f) presents $\sigma_{x,L}^2(\omega_{\text{Fourier}})$. The region I is dominated by the tunneling mode $|1,3,0\rangle_S \rightleftharpoons |1,2,1\rangle$ (see segment $\alpha_{3,1}$) and it is related to the wide avoided crossing α_3 [see solid boxes in Fig. 1(a)]. As the quench amplitude increases the region II appears for similar reasons as in the case of $\omega_i = 0.8$ and $\omega^2 \in (\omega_{\alpha_3}, \omega_{\alpha_2})$. Within the region $T_{\{\alpha_6 \alpha_5\}}$ the behavior of the system can be summarized as follows. For $\omega^2 > \omega_{\alpha_5}^2$, the process $|1,3,0\rangle_S \rightleftharpoons |2,2,0\rangle_S$ dominates the dynamics, while at $\omega^2 \approx \omega_{\alpha_5}^2$ the additional mode $|2,1,1\rangle_S \rightleftharpoons |2,2,0\rangle_S$ appears. Next, at $\omega_{\alpha_6}^2 \lesssim \omega^2 \lesssim \omega_{\alpha_5}^2$ the latter mode possesses two distinct frequencies, while the process $|1,3,0\rangle_S \rightleftharpoons |2,2,0\rangle_S$ possesses a higher frequency than in the case of $\omega^2 > \omega_{\alpha_5}^2$. Finally, at $\omega^2 \approx \omega_{\alpha_5}^2$ the low-amplitude mode $|2,1,1\rangle_S \rightleftharpoons |2,2,0\rangle_S$ corresponds to a single frequency and the process $|1,3,0\rangle_S \rightleftharpoons |2,2,0\rangle_S$ dominates the dynamics. Concluding, the response of the system at $T_{\{\alpha_6 \alpha_5\}}$ depends strongly on the postquench trap frequency. For $\omega^2 < \omega_{\alpha_6}^2$ a region II appears similarly to the case of $\omega_i = 0.8$ and $\omega^2 < \omega_{\alpha_3}$. For $\omega \approx 0$ two additional branches of low frequency appear, which correspond to the avoided crossings between $|1,2,1\rangle$ and $|2,1,1\rangle_S$ and between $|2,2,0\rangle$ and $|2,0,2\rangle_S$ (see segment $0_{1,1}$). These modes do not involve the major contribution to the initial state $|1,3,0\rangle_S$ and consequently possess very small amplitude (region III).

For higher interactions (here $g = 4E_R k^{-1}$), the dynamical response of the system, shown in Fig. 2(g) via $\sigma_{x,L}^2(t)$, after a quench on ω ($\omega_i^2 = 0.8 E_R^2 \hbar^{-2}$) shows a qualitatively different behavior from the case of intermediate interactions. The initial state is dominated by $|1,2,1\rangle$ and possesses significant contributions from higher band excitations, e.g., $|1,1^{(0)} \otimes 1^{(2)},1\rangle$ and $|1,2^{(1)},1\rangle$ [40]. The system is essentially unperturbed for $\omega^2 > 0.16 E_R^2 \hbar^{-2}$ and the evolution is characterized by multiple frequencies (see region II). Remarkably enough even for small quench amplitudes regions of Rabi oscillations [see Figs. 2(a), 2(c), 2(e)] are absent. Only for quenches to $\omega \approx 0$, a prominent response is observed [region T_0 in Fig. 2(g)]. Figure 2(h) presents $\sigma_{x,L}^2(\omega_{\text{Fourier}})$ where we observe (in contrast to the case of intermediate interactions) the appearance of only a few branches. The most dominant branch (denoted as b_1) refers to the tunneling mode $|1,2,1\rangle \rightleftharpoons |2,1,1\rangle_S$ while the second branch (denoted as b_2) corresponds to the process $|1,2,1\rangle \rightleftharpoons |1,3,0\rangle_S$. These tunneling modes appear due to the avoided crossing at $\omega = 0$ [see Fig. 1(b)]. Finally, the third branch (denoted as b_3) corresponds to the dipole mode $|1,2,1\rangle \rightleftharpoons |1^{(1)},2,1\rangle_S$. This dipole mode is induced by the minor shift of the side well caused by the quench and it is of single particle nature [41]. We remark here that in the case

of strong interactions the tunneling dynamics is suppressed allowing the dipole mode to possess a prominent role in the course of the evolution (see branch b_3).

A natural next step is to investigate whether abrupt quenches can be used for state preparation. To achieve this goal let us examine the occupation of specific number states, i.e., $N\{|\vec{n}\rangle\}(t) = |\langle \vec{n}|\Psi(t)\rangle|^2$ during the evolution within the above-mentioned dynamical regions (see also Fig. 2). Figures 3(a)–3(d) show the dynamics of a system initialized in the ground state ($\omega_i^2 = 0.8 E_R^2 \hbar^{-2}$, $g = 1E_R k^{-1}$) dominated by the number state $|0,4,0\rangle$ while in Figs. 3(e), 3(f) we consider the case ($\omega_i^2 = 0.56 E_R^2 \hbar^{-2}$, $g = 1E_R k^{-1}$) in which the $|1,3,0\rangle_S$ possesses the dominant contribution to the ground state. Figure 3(a) shows $N\{|\vec{n}\rangle\}(t)$ for a quench within the region I and near the avoided crossing α_1. A population transfer from the number state $|0,4,0\rangle$ to $|1,3,0\rangle_S$ (see segment $\alpha_{1,1}$ in Table I) following Rabi oscillations is observed. Additional contributions stemming mainly from the state $|2,2,0\rangle_S$ are negligible. On the other hand, Fig. 3(b) presents $N\{|\vec{n}\rangle\}(t)$ for a quench within the region T_{α_2}. The dominant tunneling process corresponds to $|0,4,0\rangle \rightleftharpoons |1,2,1\rangle$ (see segment $\alpha_{2,1}$), while the additional high-frequency tunneling modes $|1,3,0\rangle_S \rightleftharpoons |0,4,0\rangle$, $|1,3,0\rangle_S \rightleftharpoons |1,2,1\rangle$ coexist. As a consequence $|1,3,0\rangle_S$ possesses a significant occupation during the dynamics. Figure 3(c) shows $N\{|\vec{n}\rangle\}(t)$ for a quench within the region T_{α_3}. The main population transfer takes place between the number states $|0,4,0\rangle$ and $|2,2,0\rangle_S$ (see segment $\alpha_{3,1}$). The influence of additional contributions to the initial state is smaller because: (i) the frequency of the main tunneling mode $|0,4,0\rangle \rightleftharpoons |2,2,0\rangle_S$ is much lower than the frequency of the tunneling modes that couple the dominant state $|0,4,0\rangle$ with $|1,3,0\rangle_S$ and $|1,2,1\rangle$ and (ii) the tunneling mode $|1,3,0\rangle_S \rightleftharpoons |1,2,1\rangle$ (see segment $\alpha_{3,1}$) is pronounced due to the wide avoided crossing α_3. Figure 3(d) presents $N\{|\vec{n}\rangle\}(t)$ for a quench within the region T_{α_4}. We observe that the main population transfer takes place between the number states $|0,4,0\rangle$ and $|2,1,1\rangle_S$. The frequency of the corresponding tunneling mode (see segment $\alpha_{4,1}$) is much lower compared to the other cases shown in Fig. 3 and also compared to the remaining tunneling processes, e.g., $|1,3,0\rangle_S \rightleftharpoons |2,2,0\rangle_S$, that appear in Fig. 3(d). Figure 3(e) shows $N\{|\vec{n}\rangle\}(t)$ for a system initialized at $\omega_i^2 = 0.56 E_R^2 \hbar^{-2}$ and following a quench within the region T_{α_3}. In this case, Rabi oscillations between the number states $|1,3,0\rangle_S$ and $|1,2,1\rangle$ (see segment $\alpha_{3,1}$) are observed. Finally, Fig. 3(f) illustrates $N\{|\vec{n}\rangle\}(t)$ (same initial state) for a quench within the region $T_{\{\alpha_6 \alpha_5\}}$. Here, there are three dominant states, namely $|1,3,0\rangle_S$, $|2,2,0\rangle_S$, and $|2,1,1\rangle_S$, which are coupled via the tunneling modes $|1,3,0\rangle_S \rightleftharpoons |2,2,0\rangle_S$ and $|2,2,0\rangle_S \rightleftharpoons |2,1,1\rangle_S$ (see segment $\{\alpha_6 \alpha_5\}_1$). The total state of the system $|\Psi(t)\rangle$ is dominated within different time intervals by each of the above-mentioned number states. Concluding from the above, we note that it is possible to employ an abrupt quench of the trap frequency and achieve state preparation to one of the number states $|1,3,0\rangle_S$, $|1,2,1\rangle$, $|2,2,0\rangle_S$, and $|2,1,1\rangle_S$, with an adequate population $|\langle \vec{n}|\Psi(t)\rangle|^2 \geqslant 0.6$ (see the vertical dashed lines in Fig. 3) by choosing properly the total evolution time. This implies that multimode evolution can be used for state preparation, as long as, the frequency of the desired transition is much lower than the competing population transfer processes during the dynamics.
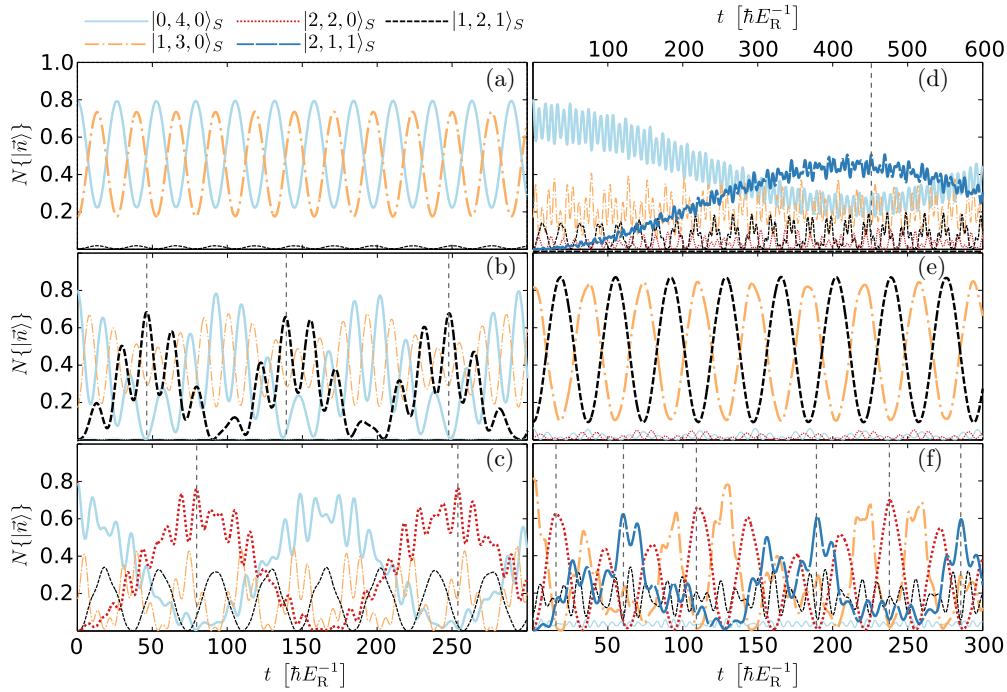
FIG. 3. Evolution of the dominant number state populations [see the legend above (a)] for $N = 4$ interacting bosons ($g = 1 E_R k^{-1}$) confined in a triple well with additional harmonic confinement ($\omega_i^2 = 0.8 E_R^2 \hbar^{-2}$). The dynamics is induced via a quench of the trap frequency to (a) $\omega^2 = 0.745 E_R^2 \hbar^{-2}$ (region I), (b) $\omega^2 = 0.58 E_R^2 \hbar^{-2}$ (region T_{α_2}), (c) $\omega^2 = 0.48 E_R^2 \hbar^{-2}$ (region T_{α_3}), and (d) $\omega^2 = 0.385 E_R^2 \hbar^{-2}$ (region T_{α_4}). Note that the scaling of the time axis in (d) is different from the other cases and appears on top of the figure. The evolution of the number state populations is also shown for a quench from $\omega_i^2 = 0.56 E_R^2 \hbar^{-2}$ to (e) $\omega^2 = 0.48 E_R^2 \hbar^{-2}$ (region I) and (f) $\omega^2 = 0.265 E_R^2 \hbar^{-2}$ (region $T_{\{\alpha_6 \alpha_5\}}$). For the identification of the different regions see Fig. 2.

To examine the dependence of the intensity of the dynamical processes on the quench amplitude, we employ $\Delta_T \{\sigma_{x,L}^2\}$ [see Eq. (II C)] being a measure of the time-averaged dynamical response, which depends solely on the parameters of the system. Figure 4 presents $\Delta_T \{\sigma_{x,L}^2\}$ as a function of the postquench trap frequency ω^2 for different values of the relevant physical parameters.

Figure 4(a) exhibits $\Delta_T \{\sigma_{x,L}^2\}$ with varying quench amplitude for different interaction strengths g. In the noninteracting case [see also Fig. 2(a)] the mean response of the system after a quench of the trap frequency is close to zero for a wide range of final trapping frequencies ($\omega^2 > 0.08 E_R^2 \hbar^{-2}$). However, for large quench amplitudes ($\omega^2 < 0.08 E_R^2 \hbar^{-2}$) the mean response increases strongly as the state $|\phi_c^{(0)}\rangle$ couples to the state $(|\phi_\ell^{(0)}\rangle + |\phi_r^{(0)}\rangle)/\sqrt{2}$. For the case of intermediate interactions ($g = 1 E_R k^{-1}$) and initial trap frequency $\omega_i^2 = 0.8 E_R^2 \hbar^{-2}$ [see also Fig. 2(c)] we observe, as expected, that the different regions of dynamical response (i.e., I, II, III, T_C) yield a distinct averaged response. In particular, for quenches within the region I the mean response of the system increases until it reaches its maximum value at $\omega_{\alpha_1}^2$. For $\omega^2 < \omega_{\alpha_1}^2$ the mean response of the system decreases. The T_{α_2} region appears as a peak in $\Delta_T \{\sigma_{x,L}^2\}$ because the interwell tunneling mode $|0,4,0\rangle \rightleftharpoons |1,2,1\rangle$ becomes resonant. For $\omega_{\alpha_3}^2 < \omega^2 < \omega_{\alpha_2}^2$ the first region of type II appears and $\Delta_T \{\sigma_{x,L}^2\}$ exhibits a local minimum. As $\omega^2 \sim \omega_{\alpha_3}^2$ the mean response increases (at the T_{α_3} region) exhibiting a narrow peak followed by a region II where the response is minimized. This process is repeated

for $\omega^2 \sim \omega_{\alpha_4}^2$ within the region T_{α_4}. The response peak at T_{α_4} is much narrower compared to the peaks in regions T_{α_3} and T_{α_2} since the resonant tunneling process $|0,4,0\rangle \rightleftharpoons |2,1,1\rangle_S$ is of third order. Furthermore, the mean response of the system remains small for $\omega^2 < \omega_{\alpha_4}^2$, with the only remarkable feature being the slightly increased response observed in region III.

For $g = 1 E_R k^{-1}$ and $\omega_i^2 = 0.56 E_R^2 \hbar^{-2}$ [see also Fig. 2(e)] a different overall dynamical response is observed. The region of type I exhibits a similar behavior as for $\omega_i^2 = 0.8 E_R^2 \hbar^{-2}$ but in this case the region II follows the region I for decreasing ω^2 without the appearance of a T region. For $\omega^2 \approx \omega_{\alpha_5}^2$, an increase in the mean response is observed as the system approaches the $T_{\{\alpha_6 \alpha_5\}}$ region. In contrast to the other T_C regions the $T_{\{\alpha_6 \alpha_5\}}$ covers a wide range of trapping frequencies ω^2 and exhibits a response peak at $\omega^2 = \omega_{\alpha_5}^2$ due to the tunneling mode $|1,3,0\rangle_S \rightleftharpoons |2,2,0\rangle_S$ (see wide part of the crossing $\{\alpha_6 \alpha_5\}$). Finally, for larger quench amplitudes the response is minimized and increases slightly only at $\omega = 0$ within the region III. For high interactions ($g = 4 E_R k^{-1}$) and initial trap frequency $\omega_i^2 = 0.8 E_R^2 \hbar^{-2}$ the dynamical response of the system is completely different from the case of intermediate interactions. The initial state of the system is dominated by $|1,2,1\rangle$ (which is also the main contribution to the ground state for $\omega^2 < \omega_i^2$). The system remains essentially unperturbed except for quenches in the proximity of $\omega \approx 0$ where an increasing response is observed due to the existence of the tunneling mode $|1,2,1\rangle \rightleftharpoons |2,1,1\rangle_S$ (see T_0 region).

Figure 4(b) presents a comparison of $\Delta_T \{\sigma_{x,L}^2\}$ obtained within the mean-field approximation and the corresponding
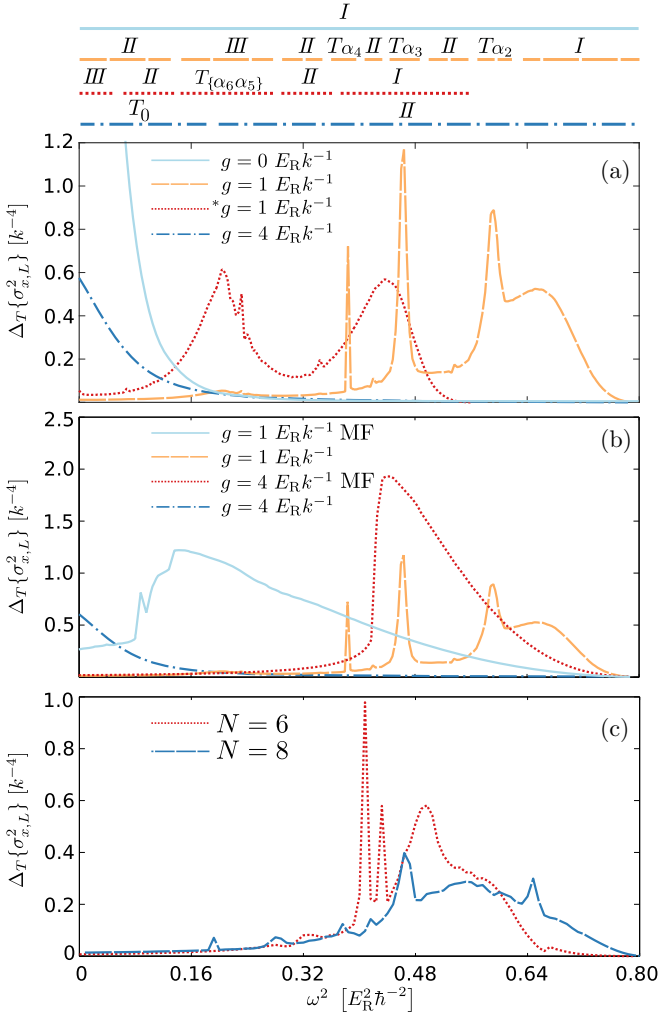
FIG. 4. $\Delta_T\{\sigma_{x,L}\}$ as a function of the postquench frequency ω^2. Comparison between (a) different interaction strengths g (see legend), (b) the mean-field (MF) and MCTDHB results (see legend), and (c) different particle numbers $N = 6, 8$ (see legend) for $g = 0.5 E_R k^{-1}$. The symbol $*$ denotes that the system is initialized in the ground state for $\omega_{i,*}^2 = 0.56 E_R^2\hbar^{-2}$ instead of $\omega_i^2 = 0.8 E_R^2\hbar^{-2}$ being used otherwise.

MCTDHB result, i.e., taking into account the correlations. As it is clearly visible the two dynamical responses differ significantly. In particular, for intermediate interactions ($g = 1$), the mean-field response of the system possesses a higher amplitude in comparison to the correlated case and continues to increase also beyond the regions T_C. Only for $\omega^2 < \omega_{\alpha_3}^2$ it finally decreases almost abruptly to a small but finite value (which is still larger than the corresponding MCTDHB value). A similar behavior is observed for higher interaction strengths. Here, the mean-field approach overestimates even more the dynamical response of the system as a consequence of the increased interparticle repulsion. We conclude that the multiple resonant behavior obtained within the correlated approach can not be captured by the mean-field approximation and consequently correlations between particles are crucial for the dynamics.

Obviously, the behavior of the system depends strongly on the particle number, since for different values of the latter the eigenstates and spectrum change overall. Figure 4(c)

presents $\Delta_T\{\sigma_{x,L}^2\}$ for the particle numbers $N = 6, 8$ and $g = 0.5 E_R k^{-1}$. Both cases show a qualitatively similar response to the $N = 4$ case presented in Fig. 4(a). Indeed, high response peaks appear also here, indicating the existence of avoided crossings in the corresponding many-body spectrum. The overall response (see, e.g., the response peaks) is altered with the number of particles, manifesting the many-body nature of the induced dynamics.

To verify the applicability of our results for larger systems, in the following section, we shall consider multiwell setups consisting of a finite optical lattice and additional harmonic confinement. Then, we shall demonstrate that the character of the diffusion dynamics induced by a quench of the frequency of the imposed harmonic trap shows similar characteristics to the triple-well case.

IV. DYNAMICS IN MULTIWELL TRAPS

Let us consider four bosons confined in a seven-well lattice with additional harmonic confinement. The system is initially prepared in the ground state for $g = 1 E_R k^{-1}$ and $\omega_i^2 = 0.56 E_R^2 k^{-2}$, where all the particles are mainly localized in the center of the trap. The initial state is dominated by Wannier number states of the form $|0,0,1,3,0,0,0\rangle_S$. Figure 5(a) shows the dynamics of the ensemble after a quench of the trap frequency to zero. We observe that even in this extreme case the atoms remain essentially localized within the region of the triple well. In particular, a small portion of the particle density tunnels away from the central well and reaches the edge of the triple-well region (where the boson gas is mainly localized) at $t \sim 100\hbar E_R^{-1}$ and subsequently expands ballistically beyond the three core sites [see Fig. 5(a)].

To explore the mean dynamical response of the system Fig. 5(b) illustrates $\Delta_T\{\sigma_{x,3}^2\}$ (where 3 stands for the integration over the three core sites) for varying final trap frequency. To perform a direct comparison with the case of the triple well we also show the mean response of the latter with equal system parameters. A similar behavior between the two cases is observed. However, we observe two deviations. First, the corresponding response peaks are slightly shifted to a lower value of ω^2. This effect can be explained by the artificial energy offset that the hard-wall boundary conditions introduce to the side wells with respect to the middle well. Indeed, this energy offset is reduced in the seven-well case. Second, an increase of $\Delta_T\{\sigma_{x,3}^2\}$ for $\omega \to 0$ is observed (see region II). This is due to the portion of atoms that expand beyond the triple-well region (the dominant tunneling mode corresponds to $|0,0,2,1,1,0,0\rangle_S \rightleftharpoons |0,1,1,1,1,0,0\rangle_S$). Indeed, as can be seen from Fig. 5(a) the unbound atomic density expands, then scatters at the hard-wall boundaries and finally reenters the triple well. This process enhances the amplitude of $\sigma_{x,3}^2$ and as a consequence the corresponding temporal variance.

To investigate the dynamical response Fig. 5(c) presents $\sigma_{x,L}^2(t)$ for different final trap frequencies. It is shown that for a quench to $\omega^2 = 0$ the portion of the density, which is unbound to the triple-well region expands ballistically. Indeed, $\sigma_{x,L}^2(t)$ after some critical value $[\sigma_{x,L}^2(t_0 = 100) \approx 5k^{-2}]$ becomes linear for a finite time interval ($100 < t < 300\hbar E_R^{-1}$). Furthermore, for quenches within the region of a response
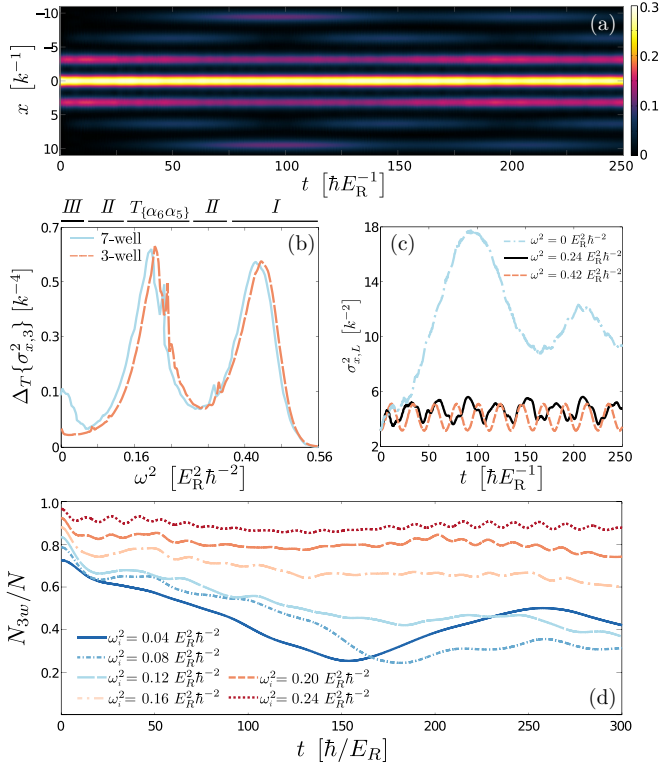
FIG. 5. (a) $\sqrt{\rho^{(1)}(x;t)}$ for $N = 4$ interacting bosons ($g = 1E_R k^{-1}$) confined in a seven-well lattice with additional harmonic confinement. The initial trap frequency is $\omega_i^2 = 0.56 E_R^2 \hbar^{-2}$ and we quench to $\omega = 0$. (b) $\Delta_T\{\sigma_{x,3w}^2\}$ with respect to the postquench ω^2 for the triple well and the seven well setup (see legend) with the same parameter values, i.e., $\omega_i^2 = 0.56 E_R^2 \hbar^{-2}$ and $g = 1E_R k^{-1}$. (c) $\sigma_{x,L}^2(t)$ for varying final trap frequency (see legend) for the seven-well setup. (d) Evolution of the density fraction within the triple-well region (N_{3w}/N) for a fifteen-well with an imposed harmonic trap. The system is initialized in the ground state with $N = 5$, $g = 1E_R k^{-1}$ for varying initial trap frequency, ω_i^2 (see legend), and the dynamics is induced by a quench to $\omega^2 = 0.016 E_R^2 \hbar^{-2}$.

peak [e.g., see region T_{α_5} at $\omega^2 \sim 0.25 E_R^2 \hbar^{-2}$ in Fig. 1(a)] or Rabi oscillations (e.g., see region I at $\omega^2 \sim 0.40 E_R^2 \hbar^{-2}$) the amplitude of $\sigma_{x,L}^2(t)$ is smaller than the critical one, thus showing the absence of a ballistically expanding fragment.

To further characterize the expansion dynamics we consider $N = 5$ bosons confined in a fifteen-well lattice potential with an imposed harmonic trap. The dynamics, shown in Fig. 5(d), is induced by a quench of the trap frequency and in particular we study quenches that refer to the same final trap frequency ($\omega^2 = 0.016 E_R^2 \hbar^{-2}$) but a different initial one. To compare the expansion dynamics we measure the fraction of the particle density within the three core sites during the dynamics, i.e., $N_{3w}(t)/N = \frac{1}{N} \int_{-3\pi/2}^{3\pi/2} dx \rho^{(1)}(x;t)$. Figure 5(d) shows that the above fragment of the particle density gets suppressed with increasing initial trap frequency. This indicates that an initially strongly confined bosonic ensemble remains after a quench of the trap frequency confined near the sites it was initially trapped into, which is a manifestation of the well-known self-trapping effect [42–44].

V. CONCLUSIONS AND OUTLOOK

We have investigated the eigenspectra and in particular the out-of-equilibrium quantum dynamics for a small ensemble of bosons confined in a lattice potential with an imposed harmonic trap. We hereby focus on the case of a strong harmonic confinement where the eigenstates become well separated and are dominated by a single Wannier number state.

In the noninteracting case, a significant tunneling dynamics is observed only for the case of a small final harmonic trapping. For intermediate interactions multiple avoided crossings with varying ω appear in the eigenspectrum, which can be exploited to reveal a rich dynamics after quenching the trap frequency. For relatively small quench amplitudes we observe Rabi oscillations caused by the wide avoided crossings between the ground and the first excited states. However, by using intermediate quench amplitudes we can utilize narrow avoided crossings involving solely excited states to selectively couple the initial state to a desired final state. The induced dynamics is characterized by multiple frequencies, one of which is particularly slow and can be used to drive the system to a desired final state. For large quench amplitudes a multimode and low-amplitude dynamical response is realized. In this case the number state with the dominant contribution to the initial state is an eigenstate of the final system (low-amplitude dynamical response), while the remaining contributions to the initial state give rise to the observed multimode dynamics. The deterministic preparation of the system in a desired Wannier number state is hindered by the fact that more tunneling modes are induced from additional contributions to the initial state. The case of stronger interparticle interactions with admixtures of a single excitation to the first excited band that do not couple in the eigenstate spectrum have been explored. The avoided crossings appear at higher trap frequencies and are narrower. The dynamics is different from the case of weak interactions, with higher band effects being more prominent and interwell tunneling being suppressed.

Let us comment on possible experimental implementations of our setup. In a corresponding ultracold gas experiment strongly interacting bosons are trapped in a one-dimensional superlattice. This superlattice can be formed by two retrore-flected laser beams from which the first one possesses a large wave number and intensity (forming each supercell) compared to the second (forming each cell of the supercell). The above-mentioned wave numbers should be commensurate. In this way, the potential landscape near the center of each supercell is similar to the one considered in the present study. Such a system may be implemented either by the use of holographic masks [45] or by the modulation of the wave number, e.g., using accordion lattices [46]. The trap frequency and the barrier height can be manipulated independently via the intensity of the lattice beams, and, finally, the interparticle interaction can be modulated via a magnetic Feshbach resonance. The corresponding static and dynamical properties of this state can then be measured with the recently developed single-site resolved imaging techniques [45,47–49]. A experimental alternative would be to prepare $2N$ fermionic ^{6}Li atoms in a microtrap [10], condense them into N Li$_2$ bosonic Feshbach molecules [50] and create a multiwell trap by switching on further microtraps [11].

The above-mentioned findings suggest that bosonic systems confined in a lattice potential with a superimposed harmonic trap can be used for state preparation in the limit of strong harmonic confinement. A natural continuation of the present work is to consider time-dependent quench protocols, such as linear quenches or pulsed sequences consisting of abrupt quenches, that may yield a substantial improvement on the state preparation, e.g., by exploiting the Landau-Zener mechanism [51–53]. Another prospect is to study the case where the parity symmetry is broken by a shift of the harmonic oscillator relative to the lattice. In this case states of opposite parity couple and one can induce transitions between states of the zeroth band and states in the first excited band. In this context novel kinds of dynamics such as Bloch-like oscillations [54–56] and the cradle mode [8,9] can be imprinted to the system. Finally, another interesting perspective is the study of nonintegrability since the many-body spectrum of the considered system shows a plethora of avoided crossings even in the few-body case. The latter might be a precursor of the advent of thermalization [57] for larger particle numbers and system sizes.

APPENDIX: COMPUTATIONAL METHOD: MCTDHB

Our approach to solve the many-body Schrödinger equation $(i\hbar\partial_t - H)\Psi(x,t) = 0$ relies on the multiconfiguration time-dependent Hartree method for bosons [24,25] (MCTDHB). MCTDHB has been applied extensively in the literature for the treatment of single species structureless bosons (see, e.g., Refs. [58–60]). The key idea of MCTDHB lies on the usage of a time-dependent (t-d) and variationally optimized many-body basis set, which allows for the optimal truncation of the total Hilbert space. The ansatz for the many-body wave function is taken as a linear combination of t-d permanents $|\vec{n}(t)\rangle$, with time-dependent weights $A_{\vec{n}}(t)$. Each t-d permanent is expanded in terms of M t-d variationally optimized single-particle functions (SPFs) $|\phi_j(t)\rangle$. For the numerical implementation the SPFs are expanded within a primitive basis $\{|k\rangle\}$ of dimension M_p. The time-evolution of the N-body wave function under the effect of the Hamiltonian $\hat{H}$ reduces to the determination of the A-vector coefficients and the SPFs, which in turn follow the variationally obtained equations of motion [24,25]. Let us note here that in the limiting case of $M = 1$, the method reduces to the t-d Gross-Pitaevski equation, while for the case of $M = M_p$, the method is equivalent to a full configuration interaction approach to the Schrödinger equation within the basis $\{|k\rangle\}$.

For our implementation we have used a sine discrete variable representation (sin-DVR) as a primitive basis for the SPFs. A sin-DVR intrinsically introduces hard-wall

boundaries at both ends of the potential. To obtain the nth many-body eigenstate we rely on the so-called improved relaxation scheme. This scheme can be summarized as follows: (i) initialize the system with an ansatz set of SPFs $\{|\phi_i^{(0)}\rangle\}$; (ii) diagonalize the Hamiltonian within a basis spanned by the SPFs; (iii) set the nth obtained eigenvector as the $A^{(0)}$ vector; (iv) propagate the SPFs in imaginary time within a finite time interval $d\tau$; (v) update the SPFs to $\{|\phi_i^{(1)}\rangle\}$; and (vi) repeat steps (ii)–(v) until the energy of the state converges within the prescribed accuracy. To study the dynamics, we propagate the wave function by utilizing the appropriate Hamiltonian within the MCTDHB equations of motion. Finally, let us remark that our implementation has been performed by employing the multilayer multiconfiguration Hartree method for bosons [61,62] (ML-MCTDHB), which reduces to MCTDHB for the case of a single bosonic species as considered here.

To verify the numerical convergence of our simulations, we impose the following overlap criteria: (i) $|\langle\Psi|\Psi\rangle - 1| < 10^{-8}$ and (ii) $|\langle\varphi_i|\varphi_j\rangle - \delta_{ij}| < 10^{-9}$ for the total wave function and the SPFs respectively. Furthermore, we increase the number of SPFs and primitive basis states observing a systematic convergence of our results. For instance, we have used $M_p = 300$, $M = 9$ for the triple well, $M_p = 560$, $M = 7$ for the seven well and $M_p = 600$, $M = 6$ for the fifteen well. In the following, we shall briefly demonstrate the convergence behavior concerning our triple-well simulations either with an increasing number of SPFs M (and fixed number of $M_p = 300$ grid points) or for a varying number of grid points M_p and a fixed number of SPFs, $M = 9$. In particular, the fulfillment of the above two conditions is presented below for two different quenches, namely from $\omega_i^2 = 0.80 E_R^2 \hbar^{-2}$ to $\omega^2 = 0.40 E_R^2 \hbar^{-2}$, $g = 1 E_R k^{-1}$ and from $\omega_i^2 = 0.80 E_R^2 \hbar^{-2}$ to $\omega^2 = 0.464 E_R^2 \hbar^{-2}$ and $g = 1 E_R k^{-1}$. For reasons of completeness, note that the first of the aforementioned quenches [see Figs. 6(a), 6(b)] lie within the region II (low dynamical response), and the second [see Figs. 6(c), 6(d)] in the region T_{α_3} (resonant dynamical response). Employing the time-evolution of our main observable, i.e., the position variance $\sigma_{x,L}^2(t)$ [see Eq. (4)], we show [see Figs. 6(a), 6(c)] that it does not alter significantly for varying number of grid points. In particular, even in the case of $M_p = 200$ the corresponding differences from the results with $M_p = 300$ [e.g., presented also in Fig. 2(d)] are negligible. Remarkably enough, the maximum deviation observed in $\sigma_{x,L}^2(t)$, for a quench lying within the region T_{α_3} [see Fig. 6(c)], calculated using 250 and 300 grid points respectively, is of the order of 2.0% for long evolution times ($t > 250$). In addition, we also present for the same quench amplitudes as above, the long time propagation of $\sigma_{x,L}^2(t)$ for different numbers of SPFs [see Figs. 1(b), 1(d)]. It is observed that in the case of $M = 3$ and $M = 6$ strong deviations from the case with $M = 9$ occur, while the cases $M = 9$ and $M = 12$ are almost indistinguishable. For instance, the maximum deviation observed in $\sigma_{x,L}^2(t)$, for a quench lying in the region T_{α_3} [see Fig. 6(c)], calculated using nine and twelve SPFs respectively, is of the order of 5.0% for long evolution times ($t > 200$). We remark that the same analysis has also been performed for the seven- and fifteen-well case (omitted here for brevity) showing a similar behavior. An additional criterion for ensuring the convergence of our simulations is the population of the lowest occupied SPF, which is kept below 0.01%.
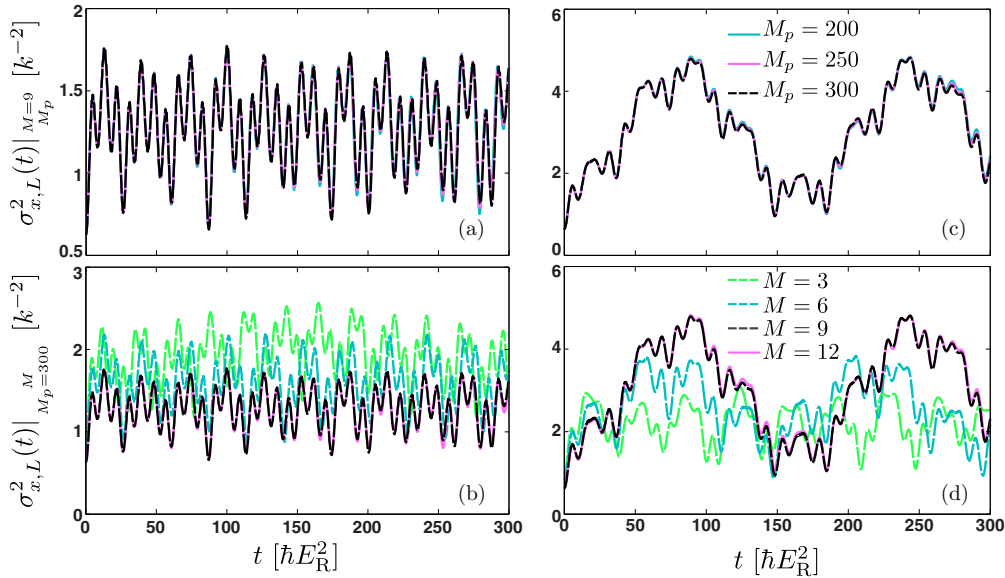
FIG. 6. $\sigma_{x,L}^2(t)$ for a quench from $\omega_i^2 = 0.80 E_{\mathrm{R}}^2 \hbar^{-2}$ to $\omega^2 = 0.40 E_{\mathrm{R}}^2 \hbar^{-2}$ and $g = 1 E_{\mathrm{R}} k^{-1}$ for (a) different number of grid points M_p and $M = 9$ SPFs, (b) different number of SPFs M and $M_p = 300$ grid points. (c), (d) The same as (a), (b) but for a quench from $\omega_i^2 = 0.80 E_{\mathrm{R}}^2 \hbar^{-2}$ to $\omega^2 = 0.464 E_{\mathrm{R}}^2 \hbar^{-2}$.

[1] I. Bloch, J. Dalibard, and W. Zwerger, Rev. Mod. Phys. **80**, 885 (2008).

[2] A. Polkovnikov, K. Sengupta, A. Silva, and M. Vengalattore, Rev. Mod. Phys. **83**, 863 (2011).

[3] M. Weidemüller, A. Hemmerich, A. Görlitz, T. Esslinger, and T. W. Hänsch, Phys. Rev. Lett. **75**, 4583 (1995).

[4] C. L. Hung, X. Zhang, L. C. Ha, S. K. Tung, N. Gemelke, and C. Chin, New J. Phys. **13**, 075019 (2011).

[5] J. P. Ronzheimer, M. Schreiber, S. Braun, S. S. Hodgman, S. Langer, I. P. McCulloch, F. Heidrich-Meisner, I. Bloch, and U. Schneider, Phys. Rev. Lett. **110**, 205301 (2013).

[6] F. Meinert, M. J. Mark, E. Kirilov, K. Lauber, P. Weinmann, M. Gröbner, A. J. Daley, and H. C. Nägerl, Science **344**, 1259 (2014).

[7] S. Fölling, S. Trotzky, P. Cheinet, M. Feld, R. Saers, A. Widera, T. Müller, and I. Bloch, Nature (London) **448**, 1029 (2007).

[8] S. I. Mistakidis, L. Cao, and P. Schmelcher, J. Phys. B: At. Mol. Opt. Phys. **47**, 225303 (2014).

[9] S. I. Mistakidis, L. Cao, and P. Schmelcher, Phys. Rev. A **91**, 033611 (2015).

[10] F. Serwane, G. Zürn, T. Lompe, T. B. Ottenstein, A. N. Wenz, and S. Jochim, Science **332**, 336 (2011).

[11] S. Murmann, A. Bergschneider, V. M. Klinkhamer, G. Zürn, T. Lompe, and S. Jochim, Phys. Rev. Lett. **114**, 080402 (2015).

[12] M. Cheneau, P. Barmettler, D. Poletti, M. Endres, P. Schauß, T. Fukuhara, C. Gross, I. Bloch, C. Kollath, and S. Kuhr, Nature (London) **481**, 484 (2012).

[13] S. S. Natu and E. J. Mueller, Phys. Rev. A **87**, 053607 (2013).

[14] D. Chen, M. White, C. Borries, and B. DeMarco, Phys. Rev. Lett. **106**, 235304 (2011).

[15] H. Elmar, R. Hart, M. J. Mark, J. G. Danzl, L. Reichsöllner, M. Gustavsson, M. Dalmonte, G. Pupillo, and H.-C. Nägerl, Nature (London) **466**, 597 (2010).

[16] K. W. Mahmud, L. Jiang, P. R. Johnson, and E. Tiesinga, New J. Phys. **16**, 103009 (2014).

[17] S. Campbell, M. A. García-March, T. Fogarty, and T. Busch, Phys. Rev. A **90**, 013617 (2014).

[18] W. Tschischik, R. Moessner, and M. Haque, Phys. Rev. A **88**, 063636 (2013).

[19] M. Rigol, G. G. Batrouni, V. G. Rousseau, and R. T. Scalettar, Phys. Rev. A **79**, 053605 (2009).

[20] G. G. Batrouni, V. Rousseau, R. T. Scalettar, M. Rigol, A. Muramatsu, P. J. H. Denteneer, and M. Troyer, Phys. Rev. Lett. **89**, 117203 (2002).

[21] V. A. Kashurnikov, N. V. Prokof'ev, and B. V. Svistunov, Phys. Rev. A **66**, 031601(R) (2002).

[22] C. Kollath, U. Schollwöck, J. von Delft, and W. Zwerger, Phys. Rev. A **69**, 031601(R) (2004).

[23] S. Wessel, F. Alet, M. Troyer, and G. G. Batrouni, Phys. Rev. A **70**, 053615 (2004).

[24] O. E. Alon, A. I. Streltsov, and L. S. Cederbaum, J. Chem. Phys. **127**, 154103 (2007).

[25] O. E. Alon, A. I. Streltsov, and L. S. Cederbaum, Phys. Rev. A **77**, 033613 (2008).

[26] M. Olshanii, Phys. Rev. Lett. **81**, 938 (1998).

[27] J. I. Kim, V. S. Melezhik, and P. Schmelcher, Phys. Rev. Lett. **97**, 193203 (2006).

[28] P. Giannakeas, F. K. Diakonos, and P. Schmelcher, Phys. Rev. A **86**, 042703 (2012).

[29] R. A. Duine and H. T. Stoof, Phys. Rep. **396**, 115 (2004).

[30] C. Chin, R. Grimm, P. Julienne, and E. Tiesinga, Rev. Mod. Phys. **82**, 1225 (2010).

[31] S. Kivelson and J. R. Schrieffer, Phys. Rev. B **25**, 6447 (1982).

[32] U. Bissbort, F. Deuretzbacher, and W. Hofstetter, Phys. Rev. A **86**, 023617 (2012).

[33] J. Enders, Master thesis, Goethe-Universität, 2014 (unpublished).

[34] W. Kohn, Phys. Rev. **123**, 1242 (1961).

[35] J. W. Abraham and M. Bonitz, Contrib. Plasma Phys. **54**, 27 (2014).

[36] M. P. A. Fisher, P. B. Weichman, G. Grinstein, and D. S. Fisher, Phys. Rev. B **40**, 546 (1989).

[37] D. Jaksch, C. Bruder, J. I. Cirac, C. W. Gardiner, and P. Zoller, Phys. Rev. Lett. **81**, 3108 (1998).

[38] We remark that at the region of the exact crossing [see the dotted box at $\omega^2 \sim 0.21 E_R^2 \hbar^{-2}$ in Fig. 1(b)], the $|2,1^{(1)},1\rangle_{S,A}$ dominated eigenstate acquires a contribution from the state $|3,0,1\rangle_{S,A}$ of the order of $\sim 10\%$. This coupling is caused by the small tilt of the side wells, which weakly breaks the corresponding parity symmetry. This, however, does not lead to any considerable alterations in the many-body spectrum.

[39] C. A. Parra-Murillo, J. Madroñero, and S. Wimberger, Phys. Rev. A **88**, 032119 (2013).

[40] States with two excited particles in the second band do not contribute significantly to the dynamics as they are energetically far from states belonging to the ground band.

[41] The dipole mode is mathematically explained by the unitary transformation $|\vec{n}\rangle(\omega_i) \xrightarrow{U} |\vec{n}\rangle(\omega)$, which maps the Wannier basis from ω_i to ω and imprints a coherentlike state to each boson initially residing in a side well.

[42] A. Smerzi, S. Fantoni, S. Giovanazzi, and S. R. Shenoy, Phys. Rev. Lett. **79**, 4950 (1997).

[43] S. Raghavan, A. Smerzi, S. Fantoni, and S. R. Shenoy, Phys. Rev. A **59**, 620 (1999).

[44] M. Albiez, R. Gati, J. Fölling, S. Hunsmann, M. Cristiani, and M. K. Oberthaler, Phys. Rev. Lett. **95**, 010402 (2005).

[45] J. F. Sherson, C. Weitenberg, M. Endres, M. Cheneau, I. Bloch, and S. Kuhr, Nature (London) **467**, 68 (2010).

[46] T. Li, H. Kelkar, D. Medellin, and M. Raizen, Opt. Express **16**, 5465 (2008).

[47] P. M. Preiss, R. Ma, M. E. Tai, J. Simon, and M. Greiner, Phys. Rev. A **91**, 041602(R) (2015).

[48] T. Fukuhara, S. Hild, J. Zeiher, P. Schauß, I. Bloch, M. Endres, and C. Gross, Phys. Rev. Lett. **115**, 035302 (2015).

[49] M. Miranda, R. Inoue, Y. Okuyama, A. Nakamoto, and M. Kozuma, Phys. Rev. A **91**, 063414 (2015).

[50] S. Sala, G. Zürn, T. Lompe, A. N. Wenz, S. Murmann, F. Serwane, S. Jochim, and A. Saenz, Phys. Rev. Lett. **110**, 203202 (2013).

[51] L. D. Landau, Phys. Z. Sowjetunion **2**, 46 (1932).

[52] C. Zener, Proc. Roy. Soc. Lond. A **137**, 696 (1932).

[53] E. C. G. Stueckelberg, Helv. Phys. Acta **5**, 370 (1932).

[54] M. Ben Dahan, E. Peik, J. Reichel, Y. Castin, and C. Salomon, Phys. Rev. Lett. **76**, 4508 (1996).

[55] O. Morsch, J. H. Müller, M. Cristiani, D. Ciampini, and E. Arimondo, Phys. Rev. Lett. **87**, 140402 (2001).

[56] S. Kling, T. Salger, C. Grossert, and M. Weitz, Phys. Rev. Lett. **105**, 215301 (2010).

[57] M. Rigol, V. Dunjko, and M. Olshanii, Nature (London) **452**, 854 (2008).

[58] A. I. Streltsov, K. Sakmann, O. E. Alon, and L. S. Cederbaum, Phys. Rev. A **83**, 043604 (2011).

[59] O. E. Alon, A. I. Streltsov, and L. S. Cederbaum, Phys. Rev. A **76**, 013611 (2007).

[60] O. E. Alon, A. I. Streltsov, and L. S. Cederbaum, Phys. Rev. A **79**, 022503 (2009).

[61] L. Cao, S. Krönke, O. Vendrell, and P. Schmelcher, J. Chem. Phys. **139**, 134103 (2013).

[62] S. Krönke, L. Cao, O. Vendrell, and P. Schmelcher, New J. Phys. **15**, 063018 (2013).